DYNAMIC PULSE BUCKLING OF A SIMPLE ELASTIC–PLASTIC MODEL INCLUDING AXIAL INERTIA

D. Karagiozova† and Norman Jones

Impact Research Centre, Department of Mechanical Engineering, The University of Liverpool,
P.O. Box 147, Liverpool L69 3BX, U.K.

Abstract—The phenomenon of dynamic elastic–plastic buckling is studied using a simple imperfection-sensitive idealized model with elastic linear work hardening springs to simulate the elastic-plastic material behaviour.

The stability theorem for autonomous systems is used to obtain the transition between stable and unstable behaviour. A step loading and three types of finite duration pressure pulses are examined. In some cases, several elastic–plastic cycles of spring deformations occur before the model shakes down to a wholly elastic behaviour.

The various results show that the effects of a pulse loading are significant even for pulses having a duration comparable with the natural period of vibration. Furthermore, the model becomes more sensitive to the influence of initial imperfections as the pulse duration decreases.

NOTATION

a	$L_2\beta/2Kr^2$
m_0, m_1	masses defined in Fig. 1(b)
L_1, L_2	lengths of members shown in Fig. 1(a)
r	L_1/L_2
t	time
u_1, u_2	displacements of springs 1 and 2 in Fig. 1, respectively
x_1, x_2	dimensionless displacements u_1/L_2 and u_2/L_2, respectively
y_0	vertical displacement in Fig. 1(b)
y	y_0/L_2
$z, \bar{z}$	$\xi/L_2, \bar{\xi}/L_2$
F_1, F_2	forces in springs 1 and 2, respectively
K, K_i	spring coefficients defined in Fig. 2
P_c	KrL_1
P_0	amplitude of external force
Q_1, Q_2, Q	defined by eqns 3(j–l)
β	non-linear spring softening characteristic at A in Fig. 1(b)
ε	ω_1^2/ω_0^2
λ	K_i/K
ξ	horizontal displacement of A in Fig. 1(b)
$\bar{\xi}$	initial imperfections indicated in Fig. 1(a)
τ	$\omega_1 t$
ω_0^2	$2K/m_0$
ω_1^2	$2Kr^2/m_1$
Δ_r	displacement at yield in springs 1 and 2
τ_0	pulse duration indicated in Fig. 3
γ	ratio of pulse duration to the natural period of horizontal vibration
$(\ )'$	$\partial(\ )/\partial\tau$
Δs	step of numerical integration.

1. INTRODUCTION

The dynamic buckling of imperfection-sensitive structures is examined by Budiansky and Hutchinson (1966), Danielson (1969), Hutchinson and Budiansky (1966), Jones (1984), Jones and dos Reis (1980), Karagiozova and Jones (1990) and Lindberg and Florence

---

† On leave from Bulgarian Academy of Sciences, Institute of Mechanics and Biomechanics, 1090 Sofia, Bulgaria.

SAS 29:10-E

(1982). Although the static buckling of structures is fairly well understood, a clear understanding of dynamic plastic buckling is lacking. However, the analysis of idealized models with simplified material properties provides some insight into this complex phenomenon.

The dynamic buckling of idealized elastic models is considered by Hutchinson and Budiansky (1966) and Danielson (1969) for a step loading having an infinite duration and by Budiansky and Hutchinson (1966) for a pulse load having a finite duration.

Dynamic buckling of the simple imperfection-sensitive model in Fig. 1 with the simultaneous influence of material plasticity and initial geometric imperfections is studied by Jones and dos Reis (1980) for a step loading. The numerical results reveal two distinct forms of dynamic response known as "direct" and "indirect" dynamic buckling which occur within specific ranges of the frequency ratio for the idealized model.

Various features of the dynamic elastic–plastic buckling of the model in Fig. 1 with $m_0 = 0$ under two pressure pulse loadings is examined by Karagiozova and Jones (1990). In particular, it was observed that, for large initial imperfections, a pulse loading causes many combinations of elastic and plastic spring deformations before instability occurs, while a step loading predicts instability within the elastic range, at least for the parameters studied.

The idealized elastic linear work hardening imperfection-sensitive model in Fig. 1 under a step loading and a finite duration pressure pulse is considered herein when retaining the influence of axial inertia (i.e. $m_0 \neq 0$).

2. BASIC EQUATIONS

The model in Fig. 1(a) is subjected to a dynamic loading $P(t)$ at point H. The various members are rigid and weightless and the only masses, m_0 and m_1, are concentrated at H and A, respectively. The unloaded model has a stress-free initial imperfection ξ, while the member FHG is constrained to remain horizontal. Member FHG and pin B are constrained to move vertically in frictionless guides. Frictionless pins are located at A, B and I and the behaviour of the softening non-linear spring at A is governed by the relation $F = \beta\xi^2$, where $\bar{\xi} + \xi$ is the total horizontal displacement at A, as indicated in Fig. 1(b). The material

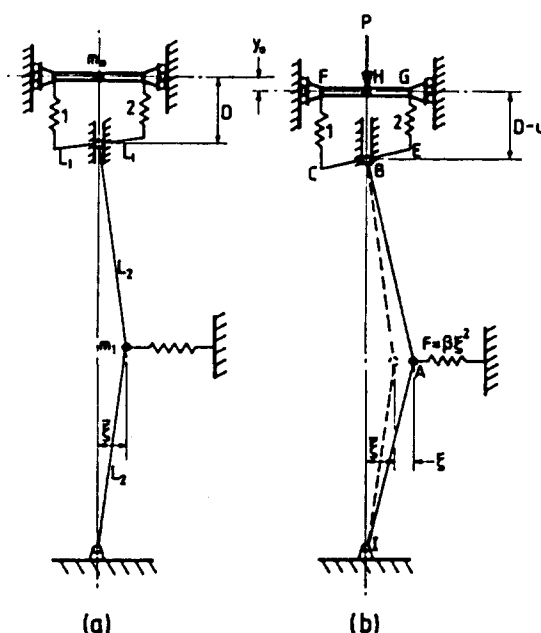(a)   (b)

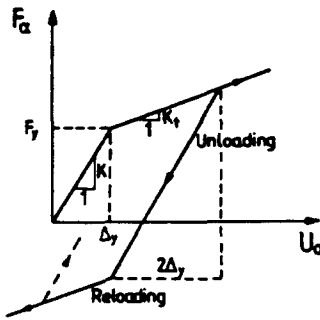Fig. 1. Simple model. (a) Initial position. (b) Deformed position.

Fig. 2. Elastic–plastic characteristics of springs 1 and 2.

behaviour of the model is simulated by springs 1 and 2 with the load-displacement characteristics shown in Fig. 2 and, for convenience, it is assumed that the springs have identical characteristics.

The dimensionless deformations of springs 1 and 2 are

$$x_1 = y - z(z + 2\bar{z}) - rz \quad \text{and} \quad x_2 = y - z(z + 2\bar{z}) + rz \qquad \text{(1a, b)}$$

respectively, and the equations of motion may be written in a dimensionless form after Jones and dos Reis (1980):

$$\varepsilon y'' + r^2(Q_1 + Q_2)/2 = r^2 Q(\tau)/2$$

and

$$z'' - (z + \bar{z})(Q_1 + Q_2) - r(Q_1 - Q_2)/2 - az^2 = 0 \qquad \text{(2a, b)}$$

where

$$y = y_0/L_2, \quad z = \xi/L_2, \quad \bar{z} = \bar{\xi}/L_2, \quad r = L_1/L_2, \quad \omega_0^2 = 2K/m_0,$$

$$\omega_1^2 = 2Kr^2/m_1, \quad \varepsilon = \omega_1^2/\omega_0^2, \quad a = L_2\beta/2Kr^2, \quad P_c = KrL_1,$$

$$Q_1 = F_1/P_c, \quad Q_2 = F_2/P_c, \quad Q = P/P_c, \quad \tau = \omega_1 t \quad \text{and} \quad ()' = \partial()/\partial\tau. \quad \text{(3a–m)}$$

The relationship between the dimensionless spring forces Q_α and the respective dimensionless displacements x_α may be expressed in the form

$$Q'_\alpha = \psi_\alpha x'_\alpha / r^2, \quad \alpha = 1, 2. \qquad \text{(4)}$$

$\psi_\alpha = 1$, when $Q_\alpha^{\min} \leq Q_\alpha \leq Q_\alpha^{\max}$, where $Q_\alpha^{\max}$ is the largest dimensionless force in the previous plastic loading of spring α, or the dimensionless yield load $(\Delta_y L_2/L_1^2)$ when no plastic flow has occurred. $Q_\alpha^{\min}$ is the smallest dimensionless force in the previous plastic reloading of spring α or the dimensionless yield load $(-\Delta_y L_2/L_1^2)$ in tension when no plastic reloading has occurred and $Q_\alpha^{\min} = Q_\alpha^{\max} - 2\Delta_y L_2/L_1^2$. $\psi_\alpha = \lambda$, when $Q_\alpha > Q_\alpha^{\max}$ and $Q'_\alpha > 0$, or when $Q_\alpha < Q_\alpha^{\min}$ and $Q'_\alpha < 0$.

Four kinds of dynamic loading are discussed in this article. Numerical results are obtained for a rectangular pulse loading [Fig. 3(a)], which is characterized by the dimensionless applied load P_0/P_c and the duration of loading τ_0, together with two triangular

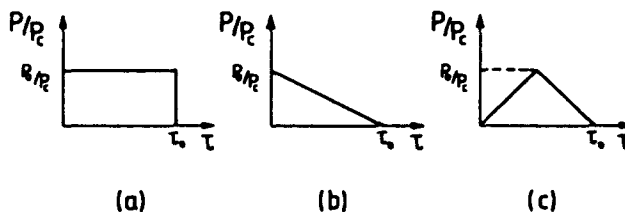(a)   (b)   (c)

Fig. 3. (a) Rectangular pulse load. (b) Triangular pulse 1. (c) Triangular pulse 2.

loadings [Figs 3(b) and 3(c)]. Comparisons are made with the step loading case, which has an unlimited duration and has been considered previously by Jones and dos Reis (1980).

Equations (2) are re-cast into a set of non-linear algebraic equations using finite-difference expressions [see Jones and dos Reis (1980)] and are solved at each time step with a standard Newton–Raphson procedure [see Carnaham et al. (1969)].

3. STABILITY OF THE MODEL

The structural response depends on the loading history of the springs because there is no one-to-one stress–strain correspondence in the presence of plastic strains according to eqns (4). Different kinds of behaviour are possible. For example, if the plastic strain increments have the same sign throughout the entire deformation process, then the total strains may become so large that the structure becomes unserviceable. On the other hand, it is also possible that after some plastic deformations during an initial phase of loading, the structural behaviour may become eventually elastic and stable [see Konig (1987)].

Let us first consider a step loading. Substituting eqns (1) and (4) into eqns (2), the governing equations of motion become

$$y'' + a_1 y + b_1 z + c_1 z^2 + d_1 = 0$$

and

$$z'' + a_2 y + b_2 z + c_2 z^2 + d_2 yz + e_2 z^3 + f_2 = 0 \qquad (5a,b)$$

where

$$a_1 = (\psi_1 + \psi_2)/(2\varepsilon), \quad c_1 = -a_1, \quad b_1 = -[(\psi_1 + \psi_2)\bar{z} + (\psi_1 - \psi_2)r/2]/\varepsilon$$

$$d_1 = -[(Q_1^0 + Q_2^0)r^2 - (\psi_1 x_1^0 + \psi_2 x_2^0) - r^2 Q_0]/(2\varepsilon) \qquad (6a-d)$$

and

$$a_2 = -(\psi_1 + \psi_2)\bar{z}/r^2 - (\psi_1 - \psi_2)/2r$$

$$b_2 = -[Q_1^0 + Q_2^0 - (\psi_1 x_1^0 + \psi_2 x_2^0)/r^2 - 2\bar{z}^2(\psi_1 + \psi_2)/r^2 - 2\bar{z}(\psi_1 - \psi_2)/r - (\psi_1 + \psi_2)/2]$$

$$c_2 = 3(\psi_1 + \psi_2)\bar{z}/r^2 + 3(\psi_1 - \psi_2)/2r - a, \quad d_2 = -(\psi_1 + \psi_2)/r^2, \quad e_2 = -d_2$$

$$f_2 = -[Q_1^0 + Q_2^0 - (\psi_1 x_1^0 + \psi_2 x_2^0)/r^2]\bar{z} - (Q_1^0 - Q_2^0)r/2 + (\psi_1 x_1^0 - \psi_2 x_2^0)/2r \qquad (7a-f)$$

and the superscript "⁰" indicates the values of the corresponding quantities when the value of ψ last changed in either of the springs.

Generally speaking, the coefficients of eqns (5a,b) are time-dependent since ψ have the values of λ or 1 depending on the active part of the force-displacement relationship in Fig. 2. Taking into account that ψ_x is a single-valued function for each part of this diagram, eqns (5a,b) may be solved and studied step-by-step at each phase of the deformation.

At every step, the coefficients of eqns (5a,b) are determined using ψ_1 and ψ_2. However, to illustrate the general procedure the behaviour of only one spring is considered below.

Assume that the external load Q_0 is sufficiently large for the spring force Q_x to be at point A in Fig. 4 when $\tau = \tau_A$. Further deformation of the model is governed by eqns (5a,b) with $\psi_x = \lambda$ and the initial conditions
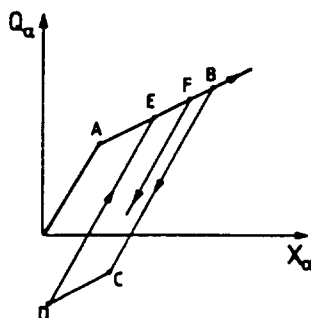

Fig. 4. Elastic–plastic loading cycles of the springs.

$$y(\tau_A) = y_A, \quad z(\tau_A) = z_A, \quad y'(\tau_A) = y'_A \quad \text{and} \quad z'(\tau_A) = z'_A. \tag{8}$$

This phase of motion with $\psi_z = \lambda$ is completed when the point B in Fig. 4 is reached. The next phase of motion has $\psi_z = 1$ and begins with the initial conditions for y, z, y' and z' at point B. It is evident that this solution procedure may be continued when passing through the points C, D, E and F in Fig. 4.

This solution procedure for eqn (5) leads to an autonomous differential equation system at every step with $\psi_z = \text{constant}$. If at every new stage of the motion the initial conditions are y^*, z^* and y'^*, z'^*, then the new variables y_1, v_1, z_1 and w_1 may be introduced as follows:

$$y_1 = y - y^*, \quad v_1 = y'_1 = v - v^*, \quad z_1 = z - z^*, \quad w_1 = z'_1 = w - w^* \tag{9}$$

where $v = y'$ and $w = z'$.

Thus, eqns (5a, b) may be rearranged as a system of four ordinary first-order differential equations

$$y'_1 = v_1, \quad v'_1 = -a_1 y_1 + b_4 z_1 - c_1 z_1^2 + d_4, \quad z'_1 = w_1$$

and

$$w'_1 = c_3 y_1 + b_3 z_1 + a_3 z_1^2 - b_2 z_1^3 - d_2 y_1 z_1 + f_4 \tag{10a-d}$$

where

$$b_4 = -(b_1 + 2az^*), \quad d_4 = -(a_1 y^* + b_1 z^* + c_1 z^{*2} + d_1), \quad a_3 = -(c_2 + 3c_2 z^*),$$

$$c_3 = -(a_2 + d_2 z^*), \quad b_3 = -(b_2 + 2c_2 z^* + d_2 y^* + 3c_2 z^{*2})$$

and

$$f_4 = -(b_2 z^* + a_2 y^* + c_2 z^{*2} + c_2 z^{*3} + d_2 y^* z^* + f_2). \tag{11a-f}$$

The singular points $(y_1^*, v_1^*, z_1^*, w_1^*)$ of eqns (10) satisfy the equations [see Davis (1962)]:

$$y'_1(v_1^*) = 0, \quad z'_1(w_1^*) = 0, \quad v'_1(y_1^*, z_1^*) = 0 \quad \text{and} \quad w'_1(y_1^*, z_1^*) = 0. \tag{12a-d}$$

In the general case, not all the singular points are real, but only the real ones are considered in this study. From the stability theorem [see Cunningham (1958)] the nature of the solution in the neighbourhood of the singular points is determined from the roots of the equation

$$\det\left[\left(\frac{\partial f_j}{\partial y_k}\right)_s - \lambda \delta_k^i\right] = 0 \tag{13}$$

where

$$\frac{dy_j}{d\tau} = f_i(y_1, y_2, \ldots, y_n), \quad i = 1, 2, \ldots, n.$$

In the case under consideration, eqn (13) becomes

$$\begin{vmatrix} -\lambda & 1 & 0 & 0 \\ -a_1 & -\lambda & b_4 - 2c_1 z_1^* & 0 \\ 0 & 0 & -\lambda & 1 \\ c_3 - d_2 z_1^2 & 0 & -3e_2(z_1^*)^2 + 2a_3 z_1^* - d_2 y_1^* + b_3 & -\lambda \end{vmatrix} = 0. \qquad (14)$$

The solution of eqns (10) is unstable even if only one root of eqn (14) has a positive real part.

The stability of the model may be determined by following the force–displacement relationship step-by-step throughout motion and studying the stability of eqns (10) with the initial conditions corresponding to the instants when either or both of the spring characteristics change from one regime to another. It is possible when the load amplitude is sufficiently large, that eqn (10) with the initial conditions for the current phase of deformation, are unstable. However, if the strain increment then changes sign during subsequent motion, it is possible that the next phase of motion is stable according to eqns (10) and the initial conditions corresponding to the instant that the strain increment changes sign.

The material model allows a sequence of elastic and plastic behaviour of the springs (Fig. 2) and, therefore, a number of loading–unloading cycles including plasticity in each complete cycle, is possible. It is of interest to enquire whether or not the model will shake down to a stable wholly elastic state after a finite number of complete cycles. In this circumstance, the displacements x_2 will be bounded as $x_2^{min} < x_2 < x_2^{max}$ with $Q_2^{min} < Q_2 < Q_2^{max}$ and stable behaviour of the model. This behaviour is possible only if the rate of the spring force increments are non-increasing functions of time during the plastic phases of motion. Every phase of motion with plastic deformation is then characterized by a decreasing force increment ΔQ_2 and after a finite number of elastic–plastic cycles the model will, therefore, shake down to a wholly elastic state. The spring force increments $\Delta Q_2^{max}/\Delta\tau$ and $|\Delta Q_2^{min}|/\Delta\tau$ are shown in Fig. 5(a). ΔQ_2^{max} and ΔQ_2^{min} are the incremental spring forces during the plastic loading and plastic reloading phases, respectively.

By changing the coefficients and the initial conditions in eqns (10), the condition for non-increasing spring force increments provides a wholly elastic solution during the last phase of motion. Different kinds of stable behaviour of the model can be established depending on the real part of the roots of eqn (14). In particular, if the roots of eqn (14) are two pairs of pure imaginary numbers, then two vortex points exist which determine limit cycles in the planes (y, y') and (z, z') for the linearized version of eqns (10). The conjugate complex roots with a negative real part determine the stable behaviour as a spiral in the corresponding planes.

In the case of a pulse loading, the above procedure is also used to study the stability of the model after the pulse is released. The initial conditions for y, z and Q_2 in eqn (10) are determined at $\tau = \tau_0$ which is shown in Fig. 3. The temporal variation of the quantities $\Delta Q_2^{max}/\Delta\tau$ and $|\Delta Q_2^{min}|/\Delta\tau$ are presented in Figs 5(b,c) for rectangular and triangular pressure pulses, respectively. These are not monotonically decreasing functions of the dimensionless time due to inertia effects, but the overall trend does decrease with time.

The spring force Q_1 during the deformation of the model under a rectangular pressure pulse is shown in Fig. 6. The increments ΔQ_1^{max} are determined from the values of Q_1 on the line AB while the pulse is active where B is the largest value of Q_1. The increments ΔQ_1^{min} while the pulse is active are determined from the values of Q_1 on the line CD. When the pulse is released at τ_0, spring 1 unloads to point B_1 and the values of Q_1^{max} are bounded by the line $C_1 D_1$, while the values of Q_1^{min} lie on line $A_1 B_1$. It transpires that the spring force increments decrease with time and Q_1^{max} and Q_1^{min} reach the constant values coinciding with the points E and F, respectively, thereby providing a wholly elastic stable behaviour of the model.

4. DYNAMIC BEHAVIOUR OF THE MODEL

The behaviour of the idealized model in Fig. 1(a) with masses m_0 and m_1 under a step loading has been studied by Jones and dos Reis (1980) with the assumption that springs 1
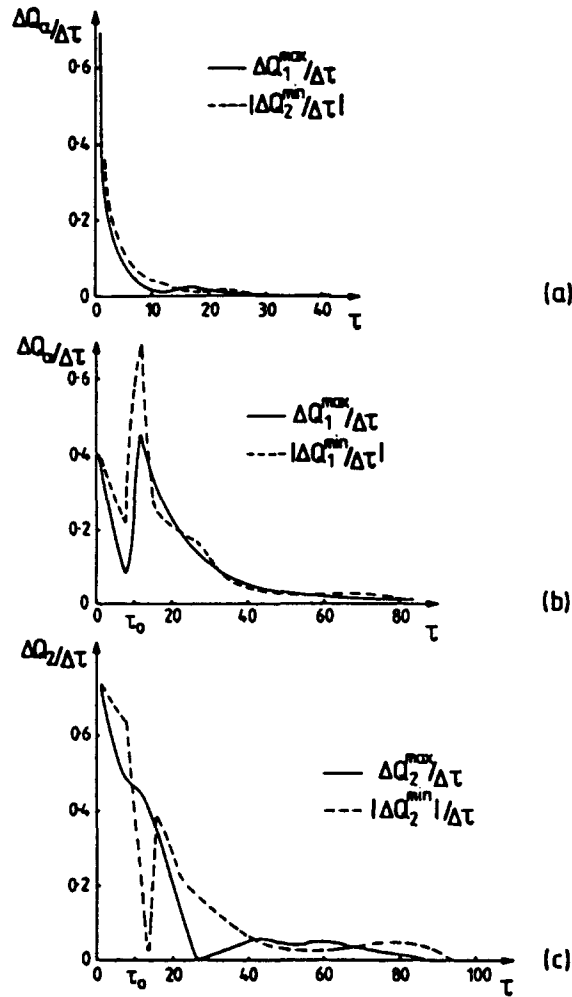
Fig. 5. (a) Spring force increments with time for a step load having $P_u/P_c = 0.72$, $\lambda = 0.75$, $\bar{s} = 0.001$, $\omega_1/\omega_0 = 0.316$, $a = 10$, $r = 1$, $\Delta_r L_2/L_1^2 = 0.268$ and $\Delta_s = 0.005$. (b) Spring force increments with time for a rectangular pulse load with $P_u/P_c = 1.0$, $\tau_0 = 10$, $\omega_1/\omega_0 = 0.55$, $\lambda = 0.75$, $\bar{s} = 0.001$, $a = 10$, $r = 1$, $\Delta_r L_2/L_1^2 = 0.268$ and $\Delta_s = 0.005$. (c) Spring force increments with time for a triangular pulse l with $P_u/P_c = 1.9$, $\tau_0 = 10$, $\omega_1/\omega_0 = 0.69$, $\lambda = 0.75$, $\bar{s} = 0.001$, $a = 10$, $r = 1$, $\Delta_r L_2/L_1^2 = 0.268$ and $\Delta_s = 0.005$.

and 2 may load elastically and plastically but unload only elastically. The possibility of spring reloading in the plastic range is considered in this article.

A stable behaviour of the model is shown in Figs 7(a, b) for an external step loading with $P_0/P_c = 0.8$ and for two different values of the frequency ratio ω_1/ω_0. For $\omega_1/\omega_0 = 0.08$, i.e. for a relatively small mass m_0, some plastic flow occurs during the first four cycles and wholly elastic vibrations $y(\tau)$ begin at $\tau \cong 7$.

The amplitude of $y(\tau)$ in Fig. 7(a) for a large mass, m_0, having $\omega_1/\omega_0 = 0.75$ is larger than that for $\omega_1/\omega_0 = 0.08$ throughout the deformation process in Fig. 7(a) even though elastic–plastic deformation occurs during the first 20 complete cycles.

It is evident from Fig. 7(b) that the horizontal displacement $z(\tau)$ is much larger for the greater value of ω_1/ω_0, while the period is slightly smaller than the period of the vertical displacement in Fig. 7(a). However, for the smaller value of ω_1/ω_0, the period of the horizontal displacements is much larger than the period of the vertical displacements.

Unstable behaviour of the model has been examined and the numerical results which are presented by Jones and dos Reis (1980) have been reproduced in the present study. Using the material model proposed herein, the same types of buckling are established and are shown in Fig. 7(c). For small values of ω_1/ω_0, a direct type of buckling is observed, while, for the larger values of ω_1/ω_0, instability occurs indirectly, as mentioned by Jones
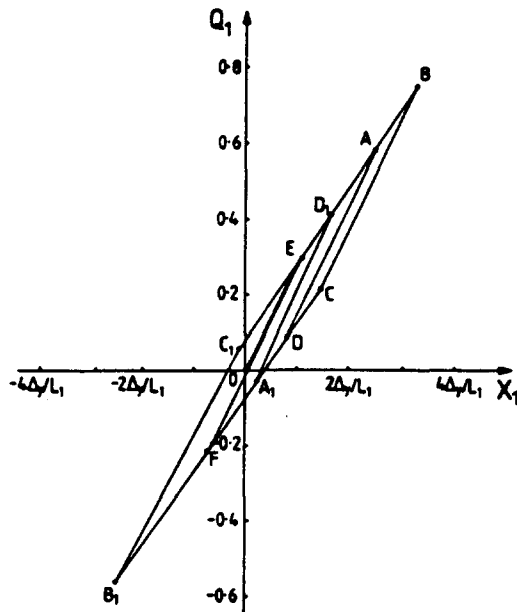
Fig. 6. Spring force Q_1 during the deformation process for a rectangular pressure pulse with $P_0/P_c = 0.8$, $\tau_0 = 5$, $\omega_1/\omega_0 = 0.316$, $\lambda = 0.75$, $\bar{z} = 0.001$, $a = 10$, $r = 1$, $\Delta_r L_2/L_1^2 = 0.268$ and $\Delta s = 0.005$.
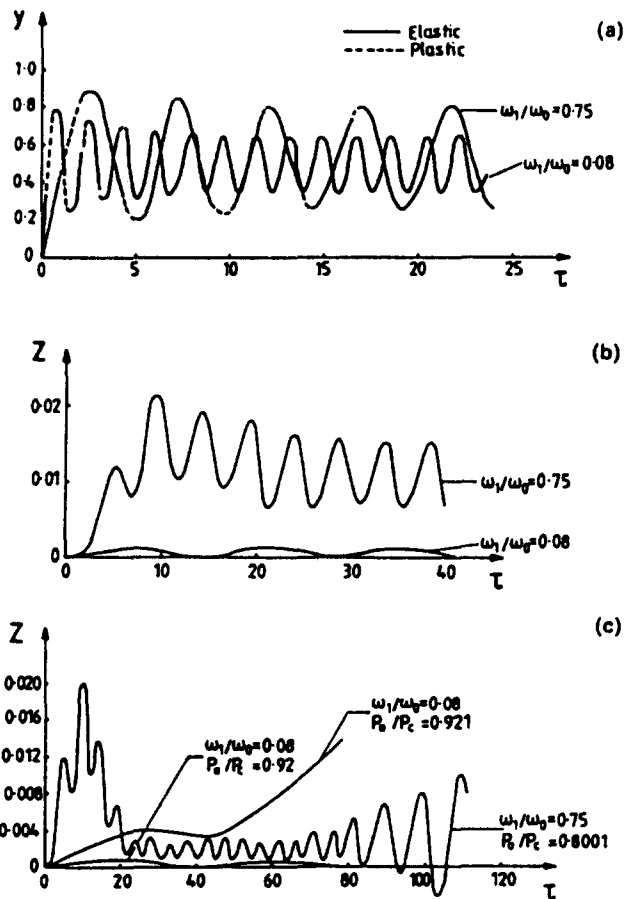

Fig. 7. Model response to an external step loading with $\lambda = 0.75$, $\bar{z} = 0.001$, $a = 10$, $r = 1$, $\Delta_r L_2/L_1^2 = 0.268$ and $\Delta s = 0.005$. (a) Axial displacement $y(\tau)$—stable behaviour with $P_0/P_c = 0.8$. (b) Horizontal displacement $z(\tau)$—stable behaviour with $P_0/P_c = 0.8$. (c) Horizontal displacement $z(\tau)$—unstable behaviour.
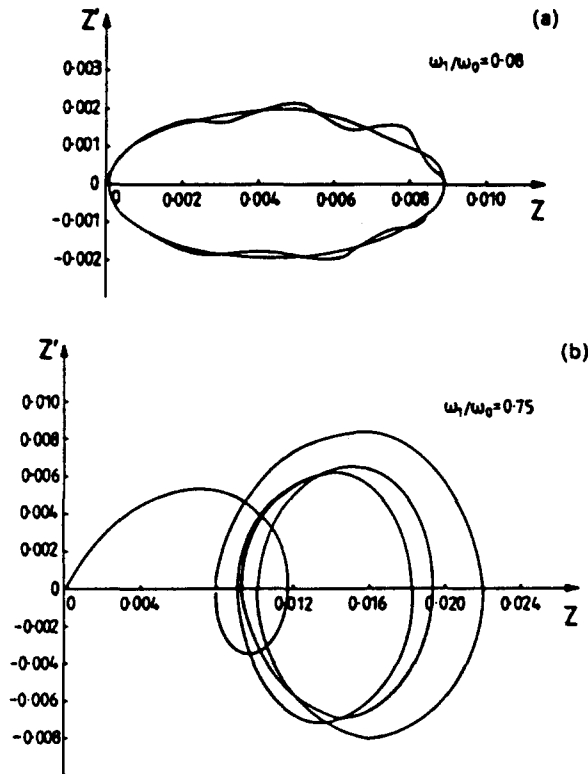
Fig. 8. Phase-plane trajectories for a step loading with $P_0/P_c = 0.8$, $\lambda = 0.75$, $\bar{z} = 0.001$, $a = 10$, $r = 1$, $\Delta_r L_2/L_1^2 = 0.268$ and $\Delta s = 0.02$.

and dos Reis (1980). Limit cycles $z'(z)$ for stable model behaviour are drawn in Fig. 8 for the frequency ratios $\omega_1/\omega_0 = 0.08$ and 0.75. The variations of the dimensionless horizontal velocities z' with the vertical and horizontal displacements for stable and unstable behaviour of the model under a step loading, are shown in Figs 9(a–d).

A comparison between the dimensionless critical loads for three different types of spring behaviour for modelling the material deformation, is presented in Fig. 10. For frequency ratios lying within the range $0 < \omega_1/\omega_0 < 0.5$, the wholly elastic behaviour predicts higher critical values of P_0/P_c than both models which include some plastic spring behaviour. However, the model which includes a plastic reloading of the springs predicts slightly larger values of P_0/P_c than the elastic–plastic case. The difference between the critical values of P_0/P_c for elastic and elastic–plastic deformations was also established for the cases when $m_0 = 0$ and $m_0 \neq 0$, and $0 < \omega_1/\omega_0 < 0.5$ by Jones and dos Reis (1980). The case of plastic reloading was not considered by Jones and dos Reis (1980), but it is observed in the present study to give only slightly larger critical loads so that it is not important from a practical viewpoint.

The elastic–plastic model predicts higher values of P_0/P_c than the wholly elastic case within the range of frequency ratios $0.5 < \omega_1/\omega_0 < 1.0$. Furthermore, the material model including plastic reloading gives much higher critical values of P_0/P_c because of the possibility of multiple elastic–plastic cycles when a significant amount of energy is absorbed in plastic deformations. The large difference between the predictions of the two elastic–plastic models when $\omega_1/\omega_0 \geqslant 0.5$ is due to the phenomenon of indirect buckling which is characterized by an important interaction between the vertical and horizontal displacements. The effect of the plastic energy absorption becomes more important because of the long times required for the development of this kind of instability.

The behaviour of the idealized model under the rectangular pressure pulse in Fig. 3(a) is shown in Fig. 11. Two complete elastic–plastic cycles are observed while the pressure pulse is active and considerable plastic reloading occurs when the pulse is released [Fig. 11(a)]. Seven complete elastic–plastic cycles then occur until the motion becomes wholly elastic at $\tau = 19.335$.
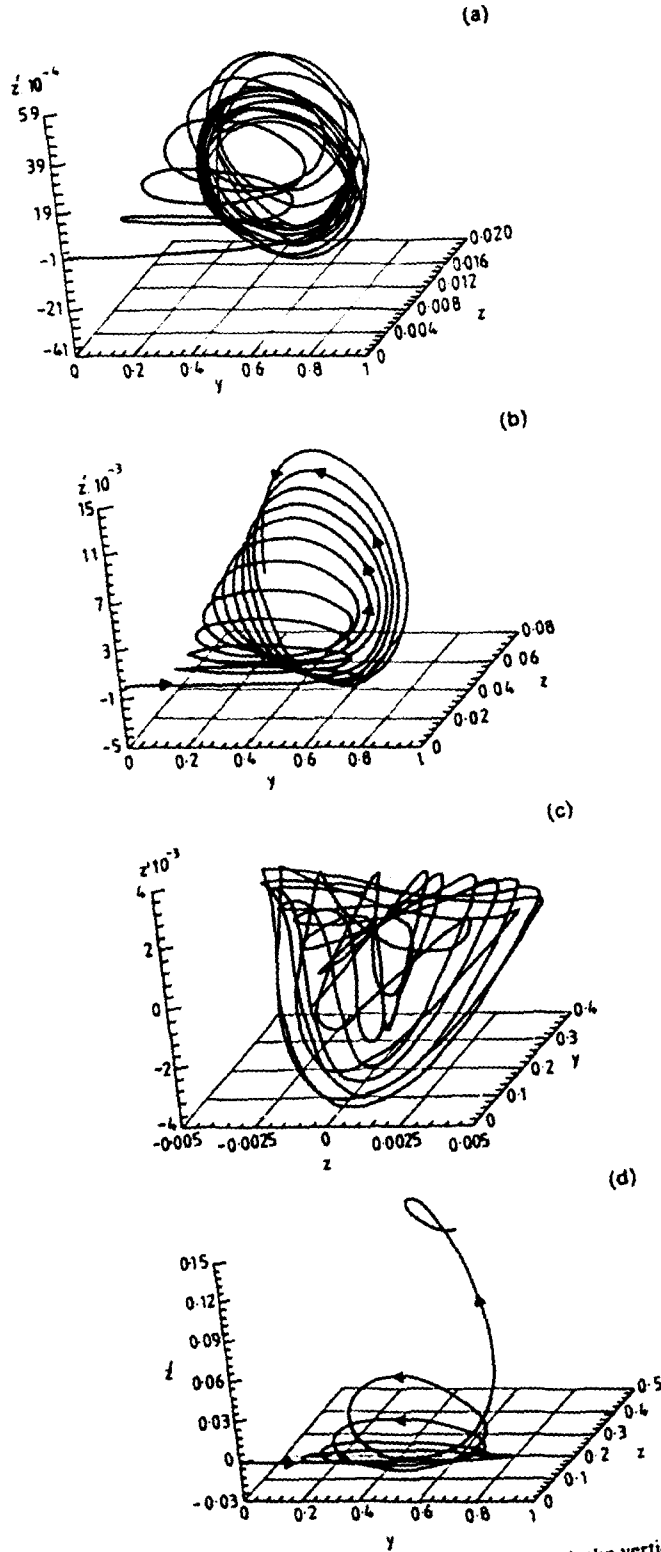
1264

(a)

(b)

(c)

(d)

Fig. 9. Variation of the dimensionless horizontal velocity z' with the vertical (y) and horizontal (z) displacements for a step loading having $\lambda = 0.75$, $\ddot{z} = 0.001$, $a = 10$, $r = 1$, $\Delta_v L_2/L_1^2 = 0.268$ and $\Delta s = 0.005$. (a) Stable behaviour of the model with $\omega_1/\omega_0 = 0.316$ and $P_0/P_c = 0.72$. (b) Unstable behaviour of the m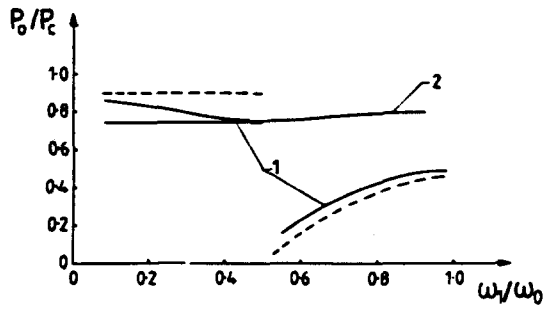odel with $\omega_1/\omega_0 = 0.316$ and $P_0/P_c = 0.748$. (c) Stable behaviour of the model with $\omega_1/\omega_0 = 0.75$ and $P_0/P_c = 0.38$. (d) Unstable behaviour of the model with $\omega_1/\omega_0 = 0.75$ and $P_0/P_c = 0.81$.

Fig. 10. Variation of dimensionless dynamic buckling load P_0/P_c with frequency ratio ω_1/ω_0 for $\lambda = 0.75$, $\bar{z} = 0.0009375$, $a = 10$, $r = 1$, $\Delta_r L_2/L_1^2 = 0.268$ and $\Delta s = 0.02$. - - - - - -, elastic model; ————, elastic–plastic model; 1, model which does not permit plastic reloading of the springs; 2, model including the possibility of plastic reloading of the springs.
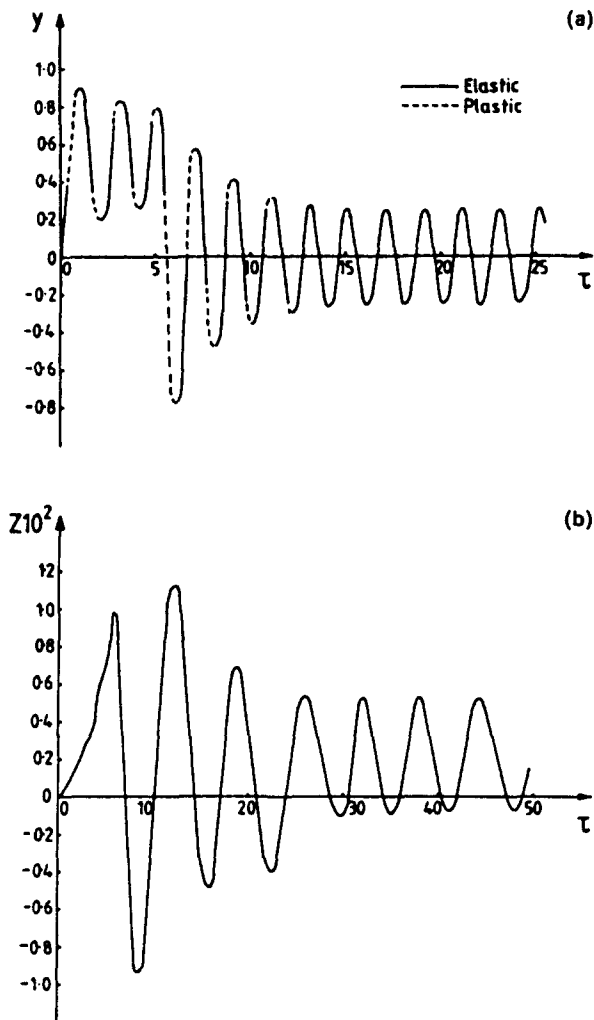
Fig. 11. Model response to a rectangular pressure pulse with $P_0/P_c = 0.8$, $\tau_0 = 5$, $\omega_1/\omega_0 = 0.316$, $\lambda = 9.75$, $\bar{z} = 0.001$, $a = 10$, $r = 1$, $\Delta_r L_2/L_1^2 = 0.268$ and $\Delta s = 0.02$.

The influence of the hardening ratio $\lambda = K_t/K$ on the critical values of P_0/P_c depend on the ratio of pulse duration to the natural period of vibration γ, as shown in Fig. 12. It is evident that the critical values of P_0/P_c depend strongly on the value of γ, so that the effect of the pressure pulse duration is significant.
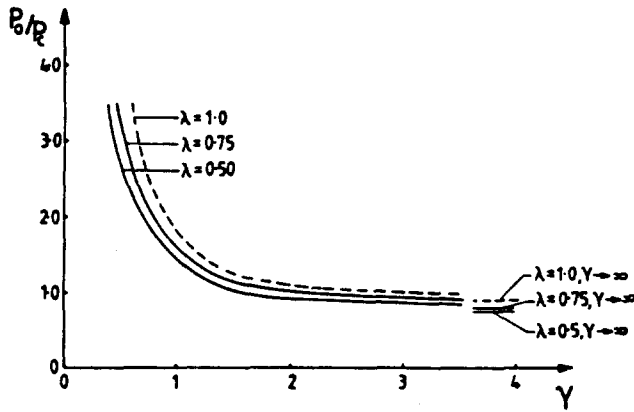
Fig. 12. Variation of the dimensionless dynamic buckling load P_0/P_c with the ratio γ for a rectangular pressure pulse having $\omega_1/\omega_0 = 0.316$, $\bar{z} = 0.001$, $a = 10$, $r = 1$, $\Delta_r L_2/L_1^i = 0.268$ and $\Delta_s = 0.02$ for three values of the ratio λ.

The initial imperfection sensitivity of the idealized model in Fig. 1 is presented in Fig. 13 for a rectangular pressure pulse loading. It is evident that the sensitivity to the initial imperfections $\bar{z}$ increases as the dimensionless duration γ decreases.

The response of the idealized model when subjected to a triangular pressure pulse [Fig. 3(b)] is shown in Fig. 14. Five complete elastic–plastic cycles occur while the pulse is active and are characterized mainly by plastic deformations due to reloading of the springs. The behaviour is almost wholly elastic after the pressure pulse loading is completed. Variation of the dimensionless horizontal velocity z' with the vertical and horizontal displacements for stable and unstable behaviour of the model under a triangular pressure pulse 1 is drawn in Figs 15(a, b). The influence of the ratio λ and the sensitivity of the critical load of the model to the initial imperfections are presented in Figs 16 and 17, respectively. It is evident that similar conclusions can be made to those for a rectangular pressure pulse.

The response of the model in Fig. 1 to a triangular pulse 2 [Fig. 3(c)] is presented in Fig. 18. The behaviour of the model during the earliest phases of motion, while the pressure pulse is active, is characterized by increasing plastic deformations. Two elastic–plastic cycles with small plastic deformations during reloading of the springs is observed after the pressure pulse is completed. The final cycle of the unloaded model in Fig. 18 is wholly elastic.

Figure 19 shows the significance of the pulse duration for the triangular pulse loading 2 on the dimensionless critical dynamic buckling loads. Even for $\gamma = 1$ the critical values are more than three times larger than the critical values for a step loading with $\lambda = 0.5$.
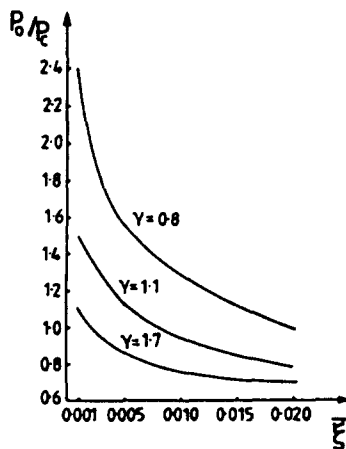

Fig. 13. Variation of the dimensionless dynamic buckling load P_0/P_c with dimensionless initial imperfections $\bar{z}$ for a rectangular pressure pulse having $\omega_1/\omega_0 = 0.69$, $\lambda = 0.75$, $\bar{z} = 0.001$, $a = 10$, $r = 1$, $\Delta_r L_2/L_1^i = 0.268$ and $\Delta_s = 0.02$ for three values of pulse ratio γ.
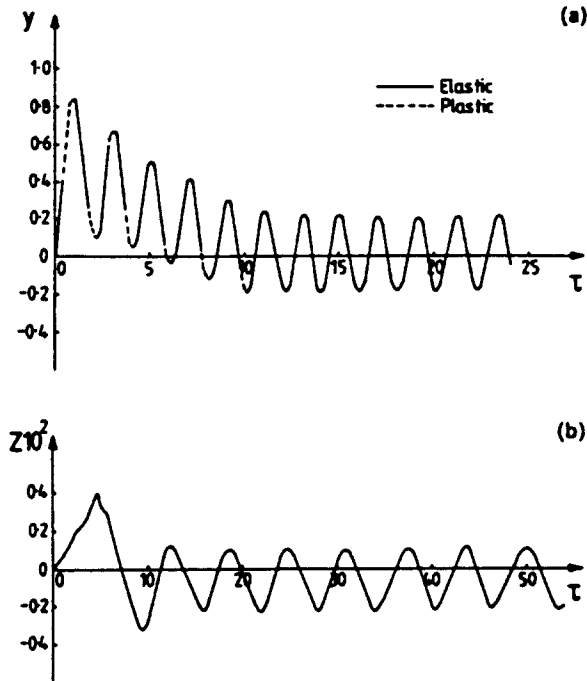
Fig. 14. Model response to a triangular pressure pulse [Fig. 3(b)] with $P_0/P_c = 0.8$, $\tau_0 = 10$, $\omega_1/\omega_0 = 0.316$, $\lambda = 0.75$, $\mathcal{Z} = 0.001$, $a = 10$, $r = 1$, $\Delta_r L_2/L_1^2 = 0.268$ and $\Delta s = 0.02$.
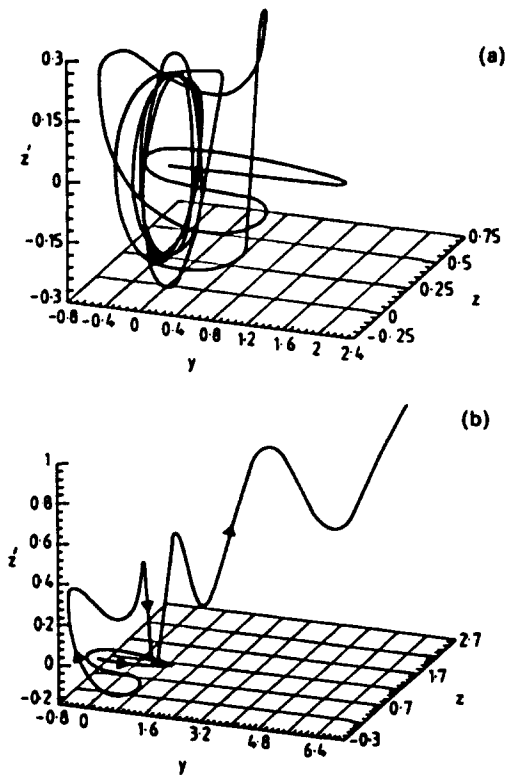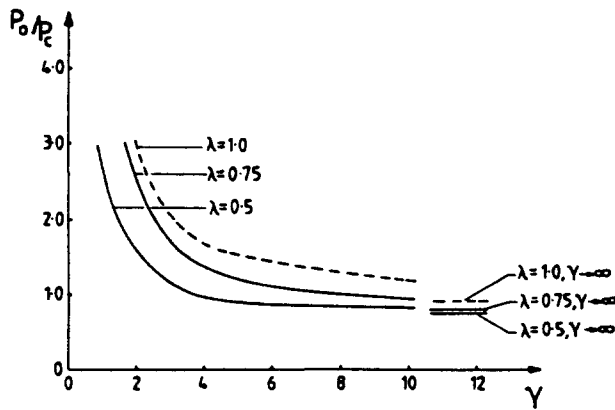

Fig. 15. Variation of the dimensionless horizontal velocity z' with vertical (y) and horizontal (z) displacements for a triangular pressure pulse 1 having $\lambda = 0.75$, $\mathcal{Z} = 0.001$, $a = 10$, $r = 1$, $\omega_1/\omega_0 = 0.69$, $\Delta_r L_2/L_1^2 = 0.268$ and $\Delta s = 0.005$. (a) Stable behaviour of the model with $P_0/P_c = 1.9$. (b) Unstable behaviour of the model with $P_0/P_c = 1.999$.

P_0/P_c

Fig. 16. Variation of the dimensionless dynamic buckling load P_0/P_c with pulse ratio γ for a triangular pressure pulse [Fig. 3(b)] having $\omega_1/\omega_0 = 0.316$, $\lambda = 0.75$, $\bar{s} = 0.001$, $a = 10$, $r = 1$, $\Delta_r L_2/L_1^2 = 0.268$ and $\Delta s = 0.02$ for three different values of the hardening ratio λ.

The initial imperfection sensitivity is presented in Fig. 20, from which it is evident that the model becomes more imperfection sensitive with decreasing pulse durations.

The dimensionless buckling pulses are $I = \gamma P_0/P_c$ and $I = \gamma P_0/2P_c$ for the rectangular and triangular loadings, respectively. A comparison between the dimensionless critical values is made in Fig. 21 for two values of λ [Fig. 21(a)] and two values of the initial imperfection $\bar{s}$ [Fig. 21(b)]. For pulses having a short duration ($\gamma < 1$) the triangular pulse 1 predicts the highest critical dimensionless values of I, while the lowest values of the critical dimensionless pulses are predicted for a rectangular shaped pressure pulse. For long duration pulses ($\gamma > 2$) the rectangular pressure pulse predicts the highest critical dimensionless pulses, while the triangular pulse 2 predicts the lowest value of I.

Figure 22 shows a comparison between the variation with γ of the critical values of the pulse amplitude P_0/P_c and the dimensionless buckling pulse $I = \gamma P_0/P_c$ for rectangular pressure pulses having $m_0 = 0$ and $m_0 \neq 0$. Equations (2) are decoupled when $m_0 = 0$ and only eqn 2(b) should be considered when taking into account that $Q = Q_1 + Q_2$. This equation is solved using the technique presented by Karagiozova and Jones (1990).

The numerical results show that axial inertia has an important influence on the critical values of the pulse amplitude P_0/P_c [Fig. 22(a)] over the whole range of pulse ratios, including $\gamma \to \infty$. The difference between the curves is particularly significant for short duration pulses ($\gamma < 0.5$). The model with $m_0 = 0$ shakes down to a wholly elastic behaviour after only one elastic–plastic cycle. However, the axial inertia of m_0 causes multiple cycles
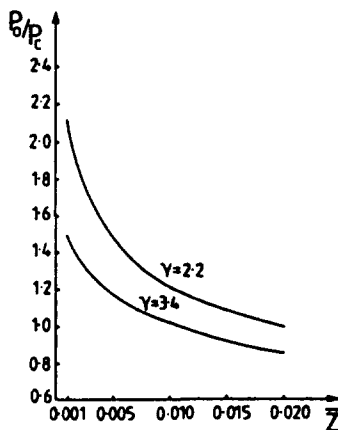
P_0/P_c

Fig. 17. Variation of the dimensionless dynamic buckling load P_0/P_c with dimensionless initial imperfections $\bar{s}$ for a triangular pressure pulse [Fig. 3(b)] having $\omega_1/\omega_0 = 0.69$, $\lambda = 0.75$, $a = 10$, $r = 1$, $\Delta_r L_2/L_1^2 = 0.268$ and $\Delta s = 0.02$ for two values of the pulse ratio γ.
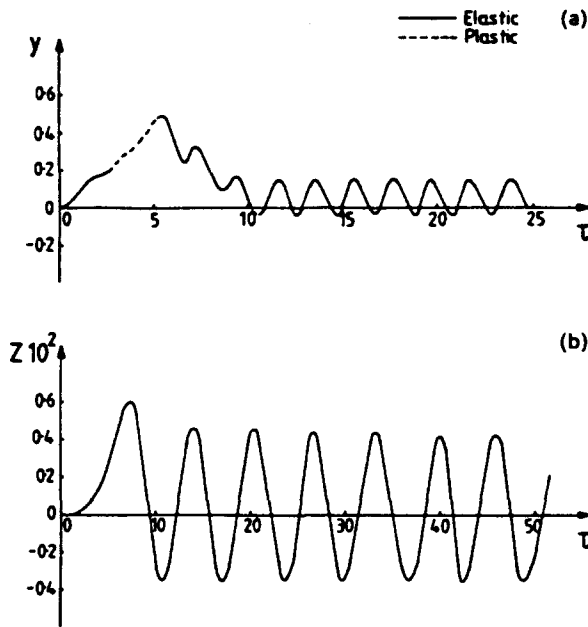
Fig. 18. Model response to a triangular pressure pulse [Fig. 3(c)] with $P_0/P_c = 0.8$, $\tau_0 = 10$, $\omega_1/\omega_0 = 0.316$, $\lambda = 0.75$, $\bar{z} = 0.001$, $a = 10$, $r = 1$, $\Delta_r L_2/L_1^2 = 0.268$ and $\Delta_s = 0.02$.

of elastic–plastic deformations during the pulse duration as well as after the pulse is released. This phenomenon allows much more energy to be absorbed during deformation which increases, therefore, the critical values of the pulse amplitudes. Furthermore, the effect of the pulse duration when $m_0 = 0$ is more significant only for short pulses ($\gamma < 1$), while in the case of $m_0 \neq 0$ this effect is important even for pulses having a duration comparable with the corresponding natural period of horizontal vibrations.

The influence of axial inertia on the critical values of the buckling pulse $I = \gamma P_0/P_c$ is shown in Fig. 22(b). The minimum value of the buckling pulse with $m_0 = 0$ occurs near $\gamma = 0.4$ whereas the minimum value is near $\gamma = 1.2$ for the buckling pulses with $m_0 \neq 0$.

5. CONCLUSIONS

The imperfection-sensitive idealized model in Fig. 1, which has elastic–plastic springs to simulate the material behaviour, was subjected to various dynamic loadings. The model response under a step loading, a rectangular pressure pulse and two types of triangular
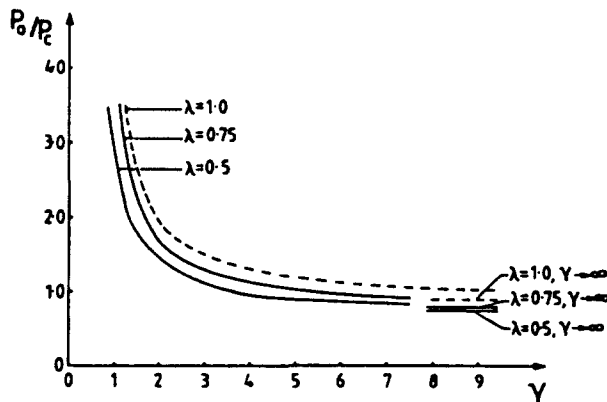

Fig. 19. Variation of the dimensionless dynamic buckling load P_0/P_c with pulse ratio γ for a triangular pressure pulse [Fig. 3(c)] having $\omega_1/\omega_0 = 0.316$, $\bar{z} = 0.001$, $a = 10$, $r = 1$ and $\Delta_r L_2/L_1^2 = 0.268$ for different values of hardening ratio λ.
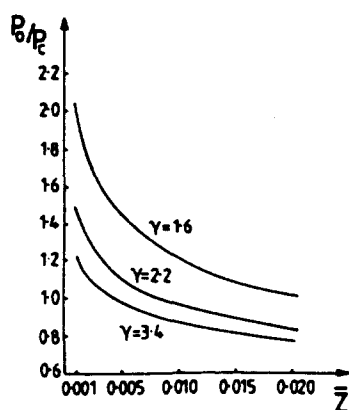
Fig. 20. Variation of the dimensionless dynamic buckling load P_0/P_c with dimensionless initial imperfections $\bar{z}$ for a triangular pressure pulse [Fig. 3(c)] having $\omega_1/\omega_0 = 0.69$, $\lambda = 0.75$, $a = 10$, $r = 1$, $\Delta, L_2/L_1^2 = 0.268$ and $\Delta s = 0.02$ for two values of the pulse ratio γ.

pressure pulse was examined using a numerical method. It is found that the stable response of the model shakes down to a wholly elastic behaviour after a certain number of elastic–plastic cycles of spring deformations for all the external loadings considered.

Higher critical values of a step loading than those reported by Jones and dos Reis (1980) are obtained when the springs are allowed to reload plastically. The difference between the two elastic–plastic models is more significant for indirect buckling in the range $0.5 < \omega_1/\omega_0 < 1.0$.
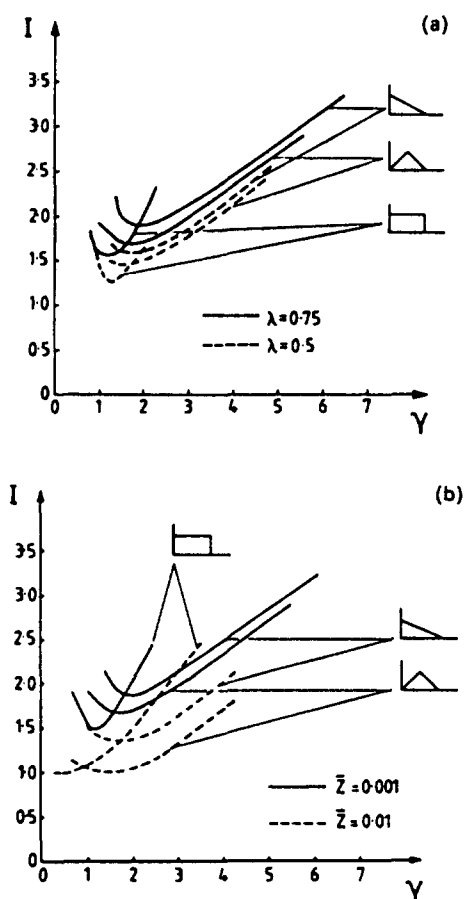

Fig. 21. Variation of the dimensionless pressure pulse I with pulse ratio γ and with $\omega_1/\omega_0 = 0.316$, $a = 10$, $r = 1$, $\Delta, L_2/L_1^2 = 0.268$ and $\Delta s = 0.02$. (a) $\bar{z} = 0.001$ and $\lambda = 0.5$, $\lambda = 0.75$. (b) $\lambda = 0.75$ and $\bar{z} = 0.001$ and $\bar{z} = 0.01$.
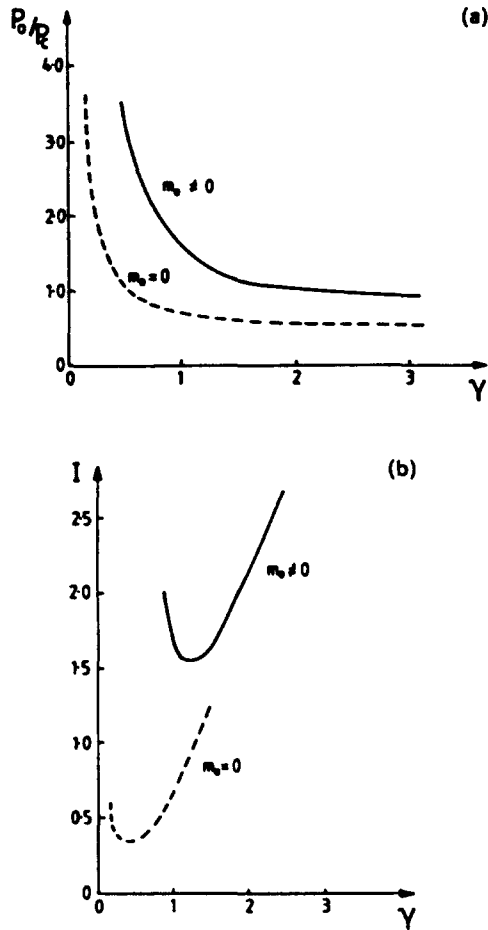
Fig. 22. Numerical results for a rectangular pressure pulse having $u = 10$, $r = 1$, $\Delta_r L_2/L_1^2 = 0.268$, $\lambda = 0.75$ and $\bar{z} = 0.001$. - - - - - -, $m_0 = 0$; ————, $\omega_1/\omega_0 = 0.316$, $\Delta s = 0.02$. (a) Variation of the dimensionless dynamic buckling load P_0/P_c with ratio γ. (b) Variation of the dimensionless rectangular pressure pulse I with pulse ratio γ.

It was observed for all the numerical calculations in this work, that the spring force rate in the plastic range, as shown in Fig. 5, always decreases for stable behaviour and increase for unstable behaviour. This could, therefore, be used as an alternative instability criterion.

The effect of the pulse loading is important even for pulses having a duration comparable with the corresponding natural period of vibration. A comparison between the various pulses shows that a rectangular pressure pulse predicts the lowest dimensionless critical pulse values I for short pulses, while, for pulses having a long duration, the lowest critical pulses are associated with a triangular pressure pulse having $P_0 = 0$ at $\tau = 0$.

The imperfection-sensitivity of the model is studied for the pressure pulse loadings and is observed to become more sensitive as the pulse duration decreases.

Axial inertia plays an important role in determining the critical values of the pulse load. The phenomenon of multiple elastic–plastic cycles due to axial inertia gives higher critical values of the pulse amplitude over the whole range of pulse ratios including $\gamma \to \infty$.

REFERENCES

Budiansky, B. and Hutchinson, J. W. (1966). Dynamic buckling of imperfection-sensitive structures. *Proceedings of the Eleventh International Congress of Applied Mechanics*. pp. 636–651. Springer, Berlin.

Carnaham, B., Luther, H. A. and Wilkes, J. O. (1969). *Applied Numerical Methods*. Wiley, New York.

Cunningham, W. J. (1958). *Introduction to Nonlinear Analysis*. McGraw-Hill, Maidenhead, U.K.

Danielson, D. A. (1969). Dynamic buckling loads of imperfection-sensitive structures from perturbation procedure. *AIAA Jl* 7(8). 1506–1510.

Davis, H. T. (1962). *Introduction to Nonlinear Differential and Integral Equations*. Dover, New York.

Hutchinson, J. W. and Budiansky, B. (1966). Dynamic buckling estimates. *AIAA Jl* 4(3), 525–530.

Jones, N. (1984). Dynamic elastic and inelastic buckling of shells. In *Developments in Thin Walled Structures* (Edited by J. Rhodes and A. C. Walker), Vol. 2, pp. 49–91. Elsevier Applied Science, Amsterdam.

Jones, N. and dos Reis, H. L. M. (1980). On the dynamic buckling of a simple elastic–plastic model. *Int. J. Solids Structures* 16, 969–989.

Karagiozova, D. and Jones, N. (1990). Dynamic buckling of a simple elastic–plastic model under pulse loading. Impact Research Centre Report No. ES/57/90, Dept. Mechanical Engineering. The University of Liverpool.

Konig, J. A. (1987). Shakedown of elastic–plastic structures. Elsevier, Amsterdam.

Lindberg, H. E. and Florence, A. L. (1982). Dynamic buckling theory and experiments. SRL Report. Also available from Martinus Nijhoff, Norwell, MA, 1987.